Univerzita Karlova

1. lékařská fakulta

Autoreferát disertační práce

FIRST FACULTY
OF MEDICINE
Charles University

Structural characterization of influenza A polymerase PA subunit domains in complex with novel inhibitors

Strukturní charakterizace komplexů domén PA podjednotky chřipkové polymerasy s novými inhibitory

Mgr. Kateřina Radilová

24. 11. 2022, Praha

Doktorské studijní programy v biomedicíně

Univerzita Karlova a Akademie věd České republiky

Obor: Molekulární a buněčná biologie, genetika a virologie (P0511D030039)

Předseda oborové rady: doc. RNDr. Dana Holá, Ph.D.

Školicí pracoviště: Ústav Organické Chemie a Biochemie Akademie Věd ČR

Školitel: RNDr. Milan Kožíšek, Ph.D.

Disertační práce bude nejméně pět pracovních dnů před konáním obhajoby zveřejněna k nahlížení veřejnosti v tištěné podobě na Oddělení pro vědeckou činnost a zahraniční styky Děkanátu 1. lékařské fakulty.

CONTENTS

ABSTRAKT 1
ABSTRACT 2
INTRODUCTION 3
RESEARCH AIMS 6
MATERIALS AND METHODS 7
RESULTS 10
CONCLUSION AND DISCUSSION 18
SUMMARY.....25
SOUHRN.....27
REFERENCES 30
PUBLICATIONS INCLUDED 32
PUBLICATIONS NOT INCLUDED 33

ABSTRAKT

RNA-dependentní RNA polymerasa viru chřipky je heterotrimerický komplex, který má zásadní roli v životním cyklu viru. Je zodpovědná za virovou replikaci a transkripci. Jedna z jejích podjednotek, PA podjednotka, interaguje s PB1 podjednotkou prostřednictvím důležité protein-proteinové interakce na své C-koncové doméně. Tato interakce, která je zprostředkovaná 310 helixem, je nutná k utvoření celého heterotrimerického komplexu. N koncová doména navíc obsahuje místo s endonukleasovou aktivitou se dvěma manganatými ionty. Obě tyto domény jsou považovány za slibné terapeutické cíle. V současnosti jsou přístupy v léčbě a prevenci chřipkového onemocnění limitované na sezónní očkování a existuje pouze několik léků, které ve velké většině cílí na jiné proteiny viru chřipky. U řady z nich však dochází k rychlému vývoji rezistentních mutací, nebo mají závažné vedlejší účinky.

Tato práce nabízí strukturní náhledy na dvě domény PA podjednotky. První část se věnuje charakterizaci a optimalizaci minimálního peptidu odvozeného z PB1 podjednotky, který interaguje s C-koncovou doménou PA podjednotky a brání jejich dimerisaci. Výsledky z této části mohou být považovány za počáteční bod pro racionální vývoj prvních inhibitorů PA-PB1 protein-proteinové interakce proti viru chřipky. V druhé polovině jsme zkoumali rostlinné chemické látky flavonoidy a sloučeniny z nich odvozené jako možné inhibitory endonukleasové domény. Pomocí rentgenové krystalografie jsme popsali vazebné módy těchto látek v aktivním místě PA podjednotky a identifikovali tak cílový protein těchto látek, které jsou hojně používané při chřipkovém onemocnění.

ABSTRACT

Influenza RNA-dependent RNA polymerase is a heterotrimeric complex and has an essential role in the life cycle of the virus. It is responsible for viral replication and transcription. One of its subunits, the polymerase acidic protein, interacts with the PB1 subunit via a crucial protein-protein interaction at its C-terminal domain. This 310 helix-mediated intersubunit interaction is required for the whole heterotrimer assembly. The N-terminal domain carries the endonuclease active site with two manganese ions. Both domains are considered promising drug targets. Current strategies to fight the influenza virus are limited to seasonal vaccines, and there are only a few anti-influenza drugs targeting mostly other viral proteins. Many used antivirals are susceptible to rapid resistance mutations development or cause severe side effects.

This thesis provides structural insights into the two domains of the PA subunit. The first part is devoted to the characterization and optimization of a PB1 derived minimal peptide interacting with the C-terminal domain. Results from this part may be considered as a starting point for the rational design of first-in-class anti-influenza inhibitors of the PA-PB1 protein-protein interaction. In the other half, we have explored the inhibitory potency of flavonoids and their derivatives against the endonuclease domain. Using X-ray protein crystallography, we have described the binding modes of those inhibitors in the PA endonuclease active site. Ultimately, we have identified the target protein of those compounds which are being broadly used as supplements during influenza viral infection.

INTRODUCTION

Influenza virus causes an acute infection of the upper respiratory system among humans and animals all around the world. The virus displays two major antigens on its surface. The first of them, hemagglutinin (HA) attaches the viral particle to the sialic acid receptor on the host cell surface, and also mediates fusion with the endosomal membrane (Cady et al., 2009). The other protein, neuraminidase (NA) releases nascent virions budding from the host cell by enzymatic cleavage of the sialic acid (Barman et al., 2004; Gottschalk, 1957). They determine further subtypes of influenza virus and so far, there are 18 subtypes of HA and 11 of NA for the influenza A virus (IAV). The IAV genetic reassortment of two influenza virus strains, results in a new subtype with mixed surface antigens (Webster et al., 1982). The newly created subtype may have a pandemic potential. The IAV is an enveloped virus containing eight segmented negative-sense single-strand ribonucleic acids (RNAs). The vRNA is wraped around viral nucleoproteins (NPs) and together with the viral RNA-dependent RNA polymerase (RdRp) form viral ribonucleoprotein complex (vRNP) (Arranz et al., 2012). Beside HA and NA proteins, the virus contains in the membrane M2 transmembrane channel, which mediates the H^+ transfer from the endosomal environment inside the endocytosed viral particle. Other viral proteins inside the viral particle execute several functions within the viral life cycle (**Figure 1.**). These include the nonstructural proteins NS1, NS2/NEP, M1, and PA-X. Finally, the IAV viral genome codes the essential RNA-dependent RNA polymerase (RdRp).

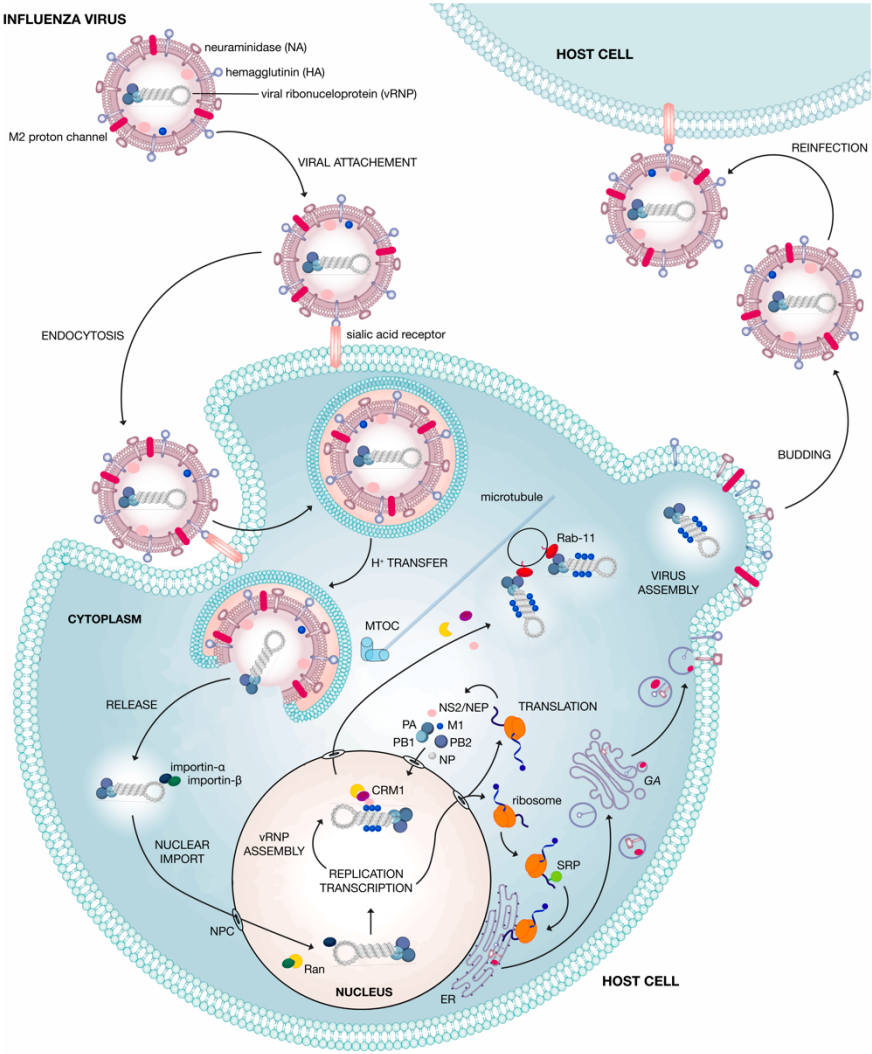

Figure 1. The IAV life cycle. Virus enters the host cell by the attachement of HA to the host sialic acid receptor. After it is endocytosed, the H^+ transfer causes conformational change of HA, membranes fuse, and viral proteins are released into the cytosol. The vRNA transciption and replication takes place in the nucleus, and the translation of viral proteins is mediated by the host proteosynthetic apparatus.

Viral proteins mature and assemble at the cell membrane. The NA cleaves of the sialic acid and nascent virus is released.

This 260 kDa-large heterotrimeric complex is composed of three subunits, the polymerase basic protein 1 (PB1), the polymerase basic protein 2 (PB2), and the PA polymerase acidic protein (PA). Their cooperation leads to the transcription and replication of the vRNA. The PA subunit is composed of two major domains, the C- terminal domain (CPA), and the N-terminal domain (NPA), connected by a long linker (**Figure 2.**). The CPA contains a hydrophobic pocket, where a 3_{10} helix of PB1 N-terminus binds. If this PA-PB1 protein-protein interaction (PPI) is disrupted, the whole heterotrimeric RdRp does not assemble. The NPA is an endonuclease, cleaving primer for viral transcription from the host mRNA, and embeds two metal ions in the active site.

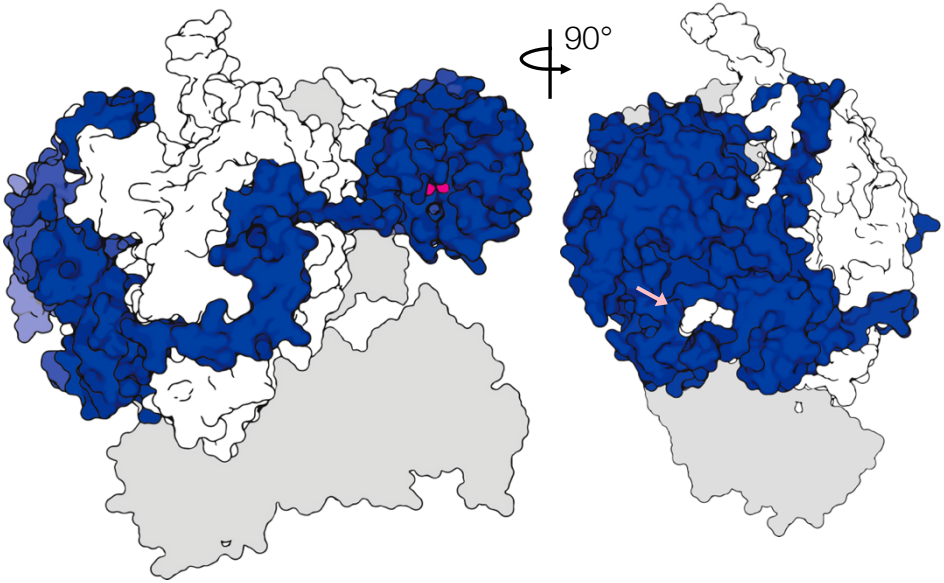

Figure 2. Two-side view on the IAV PA subunit. The PA (blue) and the PB1 (white) subunits are shown in the surface representation. The PB2 subunit is shown as gray relief for clarity. Two metal ions within the NPA endonuclease active site are pink spheres. Pink arrow indicates the PA-PB1 PPI. PDB ID: **4WSB** (Reich et al., 2014).

RESEARCH AIMS

In this work, we plan to explore two domains of the PA subunit of influenza A RNA-dependent RNA polymerase and compounds able to bind and inhibit them. Specifically, its C-terminal domain (CPA) bears an essential protein-protein interaction with another RdRp subunit, and the N-terminal domain (NPA), which has endonuclease function.

The first aim of the study is to recombinantly prepare optimized domain of 460 amino-acids, to develop a high-throughput screening assay, and to test a series of peptides for their PPI inhibitory potency. Furthermore, we want to structurally characterize the most promising peptides bound to the CPA using an X-ray protein crystallography and to utilize this for further optimization. Additionally, we intend to improve the peptide stability, intracellular delivery, and to structurally characterize whether those optimizations contribute to the binding.

Furthermore, we set to analyze the second subunit of viral polymerase, the endonuclease, with the aim to decipher the mechanism of action of flavonoids, non-specific antiviral compounds of plant origin. We plan to recombinantly express the endonuclease domain, and to develop an inhibitor-testing assay. With this assay, we want to prove or disapprove our hypothesis that molecules from a polyphenolic class flavonoids target the NPA. If so, to structurally characterize compounds in the endonuclease active site and to utilize this information for further structure-based drug design.

MATERIALS AND METHODS

Materials and methods are *in extenso* described in the attached publications.

The sequence from IAV pandemic strain A/California/07/2009 (H1N1) (GenBank accession No. CY121685.1) was used for the preparation of either CPA domain region (residues 257 –716), or the NPA domain region (residues 1 – 196), with the flexible region (residues 51 – 72) replaced by a $(GS)_4$ linker. Proteins were expressed in *E.coli* BL21(DE3)RIL and purified by gel filtration chromatography, leading to >95% purity.

The first and second generations of the CPA peptide inhibitors were tested using the newly developed AlphaScreen assay. Biotinylated peptide PB1 (1-25) was captured on streptavidin-coated donor beads (Perkin Elmer). A second solution contained GST-CPA fusion protein that bound to GSH- coated acceptor beads (Perkin Elmer). Mixtures were incubated in the dark and later mixed together with peptide inhibitors. The kinetics of the interaction was characterized by the surface plasmon resonance (SPR) experiment. Assay evaluation was performed with **PB1-0** (MDVNPTLLFLKIPA) as well as the non-inhibitory control CAI peptide (IYDPTLYGLEFD) previously used in an AlphaScreen assay for screening HIV-1 capsid assembly inhibitors (Machara et al., 2016). All experiments were performed in 25 mM Tris-HCl, pH 7.4, 150 mM NaCl, 0.05% Tween20.

The thermodynamics of **PB1-19** binding to CPA was monitored at 275.15K using a VP-ITC microcalorimeter (MicroCal Inc./Malvern Instruments Ltd., UK). Reactant solutions were prepared in 20 mM Tris-HCl, pH 7.5, containing 150 mM NaCl, 5 mM 2-mercaptoethanol, and 2% DMSO. Titrations were performed in buffers with different enthalpies of ionization (Tris-HCl, HEPES).

Purified $CPA_{257-716}$ was dialyzed into the crystallization buffer (10 mM Tris-HCl, pH 8.0, 1 mM TCEP and concentrated to 5.5 mg/ml using Amicon 30 kDa centrifugal filter units (Merck). Protein was washed with the excess of solution of 50 μM **PB1-11** (DYNPYLLFLK)/ **PB1-19** (DYNPYLLYLK) in the crystallization buffer and re-concentrated to 5.5 mg/ml in the filter unit. The protein sample monodispersity was tested on DLS instrument (Laser-Spectroscatter 201, RiNA Netzwark RNA Technologien GmbH). Crystallization experiments were performed in EasyXtal 15-well plates (QIAGEN) by the vapor-diffusion hanging drop method at 291.15 K. Crystals optimal for data collection grew in 0.1 M HEPES, pH 7.5, 35% PEG 3350. Crystals were cryoprotected by soaking in

precipitation solution supplemented with 30% ethylene glycol and flash-frozen in liquid nitrogen.

Diffraction data were collected at 100K on the MX14.1 beamline at the BESSY II electron storage ring, operated by the Helmholtz-Zentrum Berlin, Germany (Mueller et al., 2015). The dataset was processed using XDS and its graphical user interface, XDSAPP (Kabsch, 2010; Krug et al., 2012). The structure was determined by molecular replacement with the program Molrep (Vagin & Teplyakov, 2000) using protein coordinates from PDB structure **3CM8**, **6SYI** as search models (He et al., 2008; Hejdánek et al., 2021). Model refinement was performed using the program REFMAC 5.7.0032 (Murshudov et al., 1997) from the CCP4 package (Bailey, 1994) in combination with manual building and adjustments in Coot software (Emsley & Cowtan, 2004). The Molprobity server (Lovell et al., 2003) was used to evaluate the final model quality.

Both linear and bicyclic peptides were labelled with naphthofluorescein (NF) and rhodamine B (RB) to observe the peptides' intracellular delivery and early endosome escape. Peptide **PB1-11** and **PB1-19** with 3,5-bis(mercaptomethyl)benzoyl (BMB) were fused via cysteines with a short CPP motif (RRRRØF), and modified into bicyclic peptides (**PB1-11B**, **PB1-19B**) by formation of two disulfide bonds, based on Qian et al., 2017. HeLa cells were treated with 5 μM NF- and RB-labelled peptides for 2 h and visualized using confocal microscopy. Rhodamine B was captured at a wavelength of 561 nm; naphthofluorescein was captured at a wavelength of 633 nm.

The ability of bicyclic peptides to inhibit influenza virus was evaluated by the cytopathic effect reduction assay on influenza A virus (H1N1) -infected MDCK cells. To determine the effect of PB1 peptides on polymerase activity in cells, minireplicon assays were performed. In addition, the effect of bicyclization on peptide stability in human plasma was determined.

The first set of NPA-targeting compounds was tested by a newly developed high-throughput AlphaScreen assay. The biotinylated compound, structurally corresponding to the L-742,001 inhibitor, was captured on Streptavidin-coated donor beads (Perkin Elmer). Separately, GST-PA-Nter fusion protein was bound to GSH-coated acceptor beads (Perkin Elmer). Mixtures were incubated in the dark and later mixed together with compounds. All experiments were performed in 25

mM Tris-HCl, pH 7.4, 150 mM NaCl, 0.05% Tween 20, 1 mM $MnCl_2$, 10 mM $MgCl_2$, 1 mM 2-mercaptoethanol.

The endonuclease inhibitory activities of selected flavonoids were verified by in vitro cleavage of single-stranded DNA substrate M13mp18 (New England Biolabs). Each 10-mL reaction contained 1 mM GST-PA-Nter in digestion buffer (25 mM Tris-HCl, pH 7.4, 150 mM NaCl, 0.05% Tween 20, 1 mM $MnCl_2$, 10 mM $MgCl_2$, 1 mM 2- mercaptoethanol) incubated with 10 mM flavonoid and initiated by addition of 0.2 mg M13mp18 plasmid. Reactions were incubated at 310.15K for 4 h, stopped by adding 1 mL of 0.2 M EDTA, and visualized by agarose electrophoresis using a 1% agarose gel stained with GelRed.

Hexagonal bifrustum crystals of the PA-Nter subunit without ligand were obtained by the hanging-drop vapour diffusion technique at 291K by mixing 1 mL protein solution (19.2 mg/ml) with 1 mL crystallization reservoir solution (12.5% w/v MDP, 12.5% w/v PEG 1000, 12.5% w/v PEG 3350, 0.1 mM MOPS/HEPES-Na pH 7.5, 0.06 M magnesium chloride, 0.06 M calcium chloride) and 0.2 ml PA seed. Crystals appeared in 2 days and grew up to 200 mm in diameter within one week. Crystals were soaked for 2 h with luteolin, 12 h with quambalarine B, and 10 minutes with orientin in reservoir solution supplemented with 100 mM ligand solution (final 10% DMSO concentration). Crystals were flash-cooled by plunging into liquid nitrogen and were stored in liquid nitrogen.

Diffraction data were collected at 100K on a home diffractometer (MicroMax-007 HF microfocus equipped with a PILATUS 300 K detector, Rigaku). Data were processed and refined as mentioned above. The structure was solved by molecular replacement with **5CGV** as a starting model (Song et al., 2016). Molecular modelling was kindly performed by Jindřich Fanfrlík.

RESULTS

Results are *in extenso* described in attached publications.

To screen peptide inhibitors affecting protein-protein interaction between influenza polymerase PA and PB1 subunits, we developed a new assay based on an amplified luminescent proximity assay system (AlphaScreen). The interaction of the N-terminal part of PB1 peptide on donor beads with CPA on acceptor beads brings the two beads close together. If an acceptor bead coated with glutathione peptide is in proximity upon GST-CPA/PB1-biotin interaction, energy is transferred from donor to the acceptor bead, and a signal is emitted at 520 – 620 nm. In the absence of an acceptor bead due to peptide inhibition of the PA-PB1 interaction, a lower signal is produced. As expected, the interaction was blocked by a peptide corresponding to the first 14 amino acids of the PB1 N-terminus (**PB1-0**) but not by a non-inhibitory control peptide. The Z′ factor, a characteristic parameter of assay quality, was estimated to be in the range of 0.90 – 0.97, indicating an excellent assay performance and suitability for high-throughput screening. Surface plasmon resonance (SPR) experiments revealed a dissociation constant (K_d) of 23 ± 6 nM for the interaction between PB1-biotin and GST-CPA. SPR indicated specific binding of PB1-biotin to only the CPA part of the GST-CPA fusion protein. These results validated the newly developed AlphaScreen assay for screening of inhibitors of the PA-PB1 protein-protein interaction. To determine the minimal length of PB1 peptide able to inhibit the PA-PB1 protein-protein interaction, we shortened the peptide corresponding to the first 14 amino acids of the N-terminus of PB1 (**PB1-0**). Peptide **PB1-0** acted as a low nanomolar inhibitor of the PA-PB1 interaction with an IC_{50} value of 6 nM. Its truncation by up to four C-terminal amino acids led to a slight decrease in inhibition, with peptides displaying submicromolar IC_{50} values. When shortening from the N-terminus, submicromolar inhibition was observed only for peptides lacking one or two amino acids, and further truncation led to loss of inhibition potency. Next, we prepared a peptide lacking the N-terminal methionine and three amino acids at the C-terminus, but the combination of both truncations led to further reduction in inhibition, characterized by an IC_{50} of 3.4 μM. Inspired by the peptide array performed by (Wunderlich et al., 2011), we introduced two tyrosine residues into the sequence at positions 3 and 6 (**PB1-11**). These two substitutions led to substantial improvement in inhibition activity, resulting in an IC_{50} of 13 nM. Next, we

prepared a series of **PB1-11** analogs with various substitutions at hotspots, aiming to identify a variant that would maintain nanomolar affinity for CPA. Substitution of hotspot A with homo-tyrosine or *p*-carboxyphenylalanine led to affinity retention, but did not significantly improve solubility. Substitution of hotspot B with more polar residues led to a decrease in affinity, and solubility did not improve. Subsequently, we replaced the phenylalanine in hotspot C with *L*-biphenylalanine and *L*-2-naphtylalanine. The resulting peptides were strong inhibitors, but their solubility decreased. Substitution with tryptophan, *p*-carboxyphenylalanine, and tyrosine (**PB1-19**) led to improved inhibition as well as increased solubility. We selected peptide **PB1-19**, the most soluble of this series, as a candidate for thermodynamic characterization by isothermal titration calorimetry.

Titrations performed in buffers with different enthalpies of ionization yielded similar binding enthalpies (-18.8 ± 0.1 kcal mol^{-1} for Tris-HCl, -18.9 ± 0.1 kcal mol^{-1} for HEPES), indicating that under the experimental conditions there is no net proton transfer coupled to **PB1-19** binding to CPA. The dissociation constant of **PB1-19** binding to CPA was estimated to be 1.7 nM, corresponding to a Gibbs energy of binding of -12 kcal mol^{-1}. The peptide bound to CPA with a large favorable enthalpic contribution of -18.8 kcal mol^{-1} and an unfavorable entropic contribution of 6.9 kcal mol^{-1}. This dominant low enthalpy change suggests a large number of van der Waals and favorable hydrogen bonding interactions between **PB1-19** and CPA.

To evaluate whether the bindings of the modified peptides were structurally consistent with previously published structures of the PA-PB1 interface (He et al., 2008; Obayashi et al., 2008), we crystallized a complex of CPA with the peptides **PB1-11** and **PB1-19**. Crystals exhibited $P\ 2_12_12_1$ symmetry and diffracted up to 1.6 Å, and 1.9 Å respectively, and contained one CPA molecule in the asymmetric unit. Coordinates of CPA-**PB1-11**/**PB1-19** complexes were deposited with PDB accession numbers **6SYI** and **7ZPY**. The binding modes of the decapeptides in **6SYI** (DYNPYLLFLK) and **7ZPY** (DYNPYLLYLK) were nearly identical (**Figure 3.**), similarly to the native PB1 N-terminal peptide in **2ZNL**. Superposition of peptides **PB1-11** and **PB1-19** in the CPA hydrophobic pocket gave an RMSD of 0.21 Å for 81 corresponding atoms. The mutation of Phe-9 to Tyr-9 yielded two additional water-mediated hydrogen bonds with O^{γ}Ser-662 in the α13 helix and

created a water net (w1-w4) connecting Tyr-9 and Tyr-6 with $O^{\delta 1}$Asn-703 from helix α13. This resulted in the shift of residues ranging from Ala-651 (α11 helix) to Leu-694 (α12 helix) of RMSD of 0.84 Å for corresponding 332 atoms. The hydroxyl group of Tyr-3 forms a water-mediated hydrogen bond (w5) with the main chain carboxyl of Cys-415, as observed in the complex of CPA with **PB1-11**.

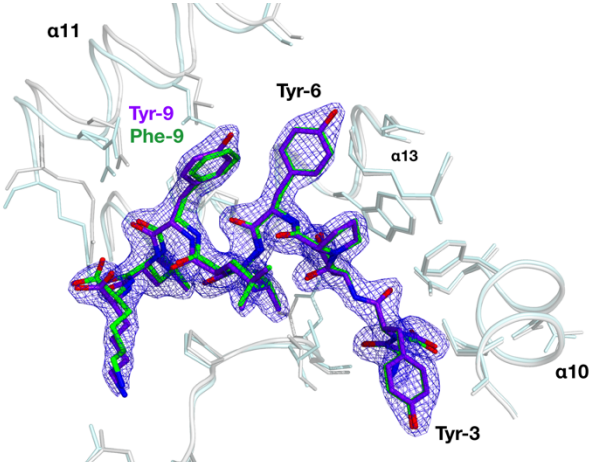

Figure 3. Close-up view on the CPA hydrophobic binding pocket with aligned peptides. Peptides **PB1-11** (green) and **PB1-19** (purple-blue) are in stick representations. Three "hotspots" (Tyr-3, Tyr-6 and Tyr-9/Phe-9) are highlighted. The 2*F*o - *F*c electron density map (contoured at 1.5σ) of **PB1-19** is shown as blue mesh

To evaluate the in vivo activity of the peptides, first we attached the cell-penetrating Tat peptide to the C-terminal, which did not impact peptide binding in vitro. The inhibitory capabilities of the peptides were evaluated with three cell-based approaches. Initially, we tested the ability of the peptides to inhibit influenza RNA polymerase in a minireplicon assay. In this assay, peptides were added to HEK293T cells co-transfected with a plasmid encoding polymerase subunits PA, PB1, and PB2 together with nucleoprotein and a luciferase reporter plasmid containing an influenza viral minigenome. The **PB1-0** inhibited viral RNA transcription only after attachment of the Tat peptide. The addition of Tat on either terminus to the **PB1-11** did not considerably improve the inhibition of influenza

RNA polymerase in the minireplicon assay. In the plaque reduction assay, MDCK cells are infected with influenza A H1N1 virus. The **PB1-11** was able to reduce the number of plaques. Attachment of Tat on either terminus did not improve the inhibition activity of **PB1-11**. Finally, MDCK cells were pretreated with the peptides prior to infection with influenza A H1N1 virus. Truncated peptide **PB1-11** was able to reduce influenza virus-induced CPE. Addition of Tat to either terminus did not improve the inhibitory activity of **PB1-0**, and the same modifications of **PB1-11** reduced inhibition. Uninfected MDCK cells tolerated all modified and unmodified peptides at concentrations up to 200 μM.

Intracellular peptide inhibitors are sensitive to degradation, rapid plasma clearance and low plasma membrane permeability. These poor pharmacokinetic properties of peptide inhibitors are challenging to overcome even using cell-penetrating peptide (CPP) sequences. Therefore, we used a recently described reversible bicyclization strategy that yields enhanced proteolytic stability and efficient escape from the early endosome into the cytosol, providing protection from proteolysis in the endosome/lysosome. Peptide **PB1-11** with 3,5-bis(mercaptomethyl)benzoyl (BMB) was fused via cysteines with a short CPP motif (RRRRØF), and modified into a bicyclic peptide by formation of two disulfide bonds. The bicyclic peptide **PB1-11B** enters cells by endocytosis and escapes from the early endosome into the cytosol, where intracellular glutathione would reduce the pair of disulfide bonds (**Figure 4.**). The released linear peptide, **PB1-21**, then inhibits the intracellular **PA-PB1** interaction. Results from AlphaScreen indicated that **PB1-21** retained inhibitory efficacy (IC_{50} = 10 nM).

To observe the peptides' intracellular delivery and escape from the early endosome into the cytosol, we labelled both linear and bicyclic peptides with naphthofluorescein (NF) and rhodamine B (RB). HeLa cells were treated with 5 μM NF- and RB-labelled peptides (**PB1-11**, **PB1-11B**) and visualized using confocal microscopy. Peptides labelled with the pH-insensitive RB were visible intracellularly across the entire pH range, giving a fluorescent signal both in cytosol and inside endosomes. The NF-labelled **PB1-11B** exhibited diffuse fluorescence only in the cytosol, as the label is pH-sensitive. The addition of a cell-penetrating sequence increased the peptide's cytosolic delivery. Compared to the linear **PB1-11**, the bicyclic **PB1–11B** showed greater fluorescence in both labelled

variants. This suggests not only increased transmembrane transport, but also enhanced escape from the early endosome.

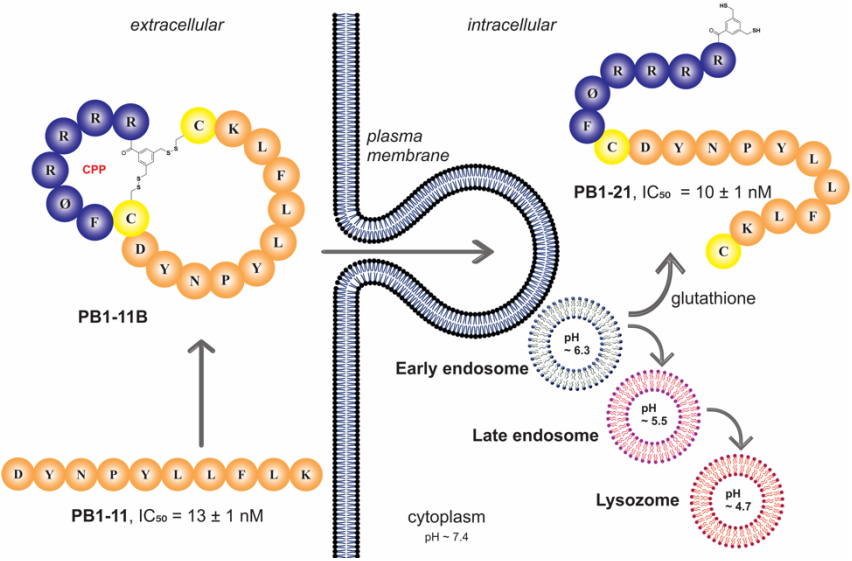

Figure 4. Bicyclic peptide strategy for efficient delivery of PB1-11 into cells.

The effect of linear peptides **PB1-11** and **PB1-19** and their bicyclic variants was evaluated with two cell-based approaches: a minireplicon assay and a CPE reduction assay. In the minireplicon assay, **PB1-11** barely inhibited RdRp (EC_{50} of 64 μM) and **PB1-19** did not have any effect. The bicyclic strategy significantly improved the properties of the peptide inhibitors in cell-based assays. **PB1–11B** showed a six-fold increase in influenza A RdRp inhibition. The **PB1–19B**, which was determined to be a low micromolar polymerase inhibitor (EC_{50} of 1 μM). To confirm the ability of bicyclic peptides to inhibit influenza virus in cell culture, we used a CPE reduction assay. MDCK cells were treated with peptides before infection with influenza A H1N1 virus. The bicyclic peptide **PB1–11B** exhibited a two-fold higher inhibitory effect than linear **PB1-11**. We observed a significant effect of bicyclic peptide delivery for **PB1–19B**, which had an EC_{50} value of 2 μM in the infectious assay. Both HEK293T and MDCK cells tolerated all peptides a

concentrations up to 100 μM. Favipiravir, baloxavir marboxil and pimodivir were used as controls. In addition, we determined the effect of bicyclization on peptide stability in human plasma. Both linear peptides, **PB1-11** and **PB1-19**, underwent rapid proteolytic degradation in human plasma with half-lives of 12 and 13 min, respectively. In contrast, bicyclic peptides **PB1–11B** and **PB1–19B** had half-lives of about 175 and 123 min, respectively.

We set to develop a new assay for screening of the PA-Nter (NPA) inhibitors based on the amplified luminescent proximity assay, AlphaScreen. The metal-binding motif of the L 742,001 was decorated with an u-biotinylated flexible linker, and this adduct was noncovalently bound to donor beads coated with streptavidin. NPA was with an N-terminal GST-tag bound to acceptor beads coated with glutathione. Anallogously to the AlphaScreen assay for the CPA, the presence of potent NPA inhibitor disrupts the binding interaction of a tethered derivative of L-742,001-like probe with NPA and reduces emission signal. An SPR analysis was performed to test the binding parameters of the L-742,001-like probe prior to its usage in the AlphaScreen experiment. The SPR results indicated binding of the modified probe to the protein, and revealed a dissociation constant (K_d) less than 9.3 nM. First set of flavonoids derivatives (83 compounds) was tested. Quercetin exhibited an IC_{50} value of 0.67 mM, validating our hypothesis linking the therapeutic effect of flavonoids to inhibition of influenza endonuclease.

To understand binding of mentioned polyols to the influenza endonuclease enzyme, we selected two compounds for X-ray crystallographic studies of protein-ligand complexes, considering inhibitory potency and aqueous solubility. Luteolin and quambalarine B were soaked into unoccupied protein crystals. The structure of NPA in complex with luteolin was refined to 2.0 Å resolution; quambalarine B was refined up to 2.5 Å, deposited to the PDB with codes **6YA5** and **6YEM**, respectively. In the final crystallographic models, each asymmetric unit consisted of one NPA molecule. Two octahedrally coordinated metal ions were embedded in the active site. Due to a strong anomalous signal observed up to 2.3 Å, we determined the proximal ion to be fully occupied by a Mn^{2+} cation. The octahedral coordination sphere is formed by the central Mn^{2+} ion, four protein atoms of $N^{\varepsilon 2}$ His-41, $O^{\delta 2}$ Asp-108, $O^{\varepsilon 2}$ Glu-119, O Ile-120, and two hydroxyl groups of luteolin. The distal cation exhibited lower anomalous scattering, in agreement with a previously reported structural analysis of NPA complexes. This indicates partial

occupation of the site with a Mg^{2+} cation, which is coordinated by $O^{\varepsilon 2}$ Glu-80, O^{δ} Asp-108, the C3' hydroxyl group of luteolin, and three water molecules (W1, W2, W3). Metal ions in enzymatically active NPA (PDB entry **5DES**) coordinate two molecules of water. In the luteolin complex, these waters are replaced with the two hydroxyl groups of the flavonoid's B ring. Clearly, binding to the endonuclease active site utilizes binding mode A. The flavone scaffold of luteolin creates van der Waals interactions within the active site pocket (**Figure 5A.**). Additionally, the hydroxyl group at position C7 creates a hydrogen bond with $O^{\varepsilon 2}$ Glu-26. Quambalarine B acts as a tridentate ligand bound to NPA via its 7,8-dihydroxynaphthoquinone moiety. The ligand affinity is improved by the ketone moiety which contributes to van der Waals interaction with water molecule in first solvation shell of protein. The rest of the ligand molecule is not engaged in direct interactions with protein residues and is oriented towards the solvent. We also attempted X-ray crystallographic characterization of a NPA complex with myricetin. However, the electron density of the flavonol was of poor quality; its position in the active site was ambiguous. Thus, we applied molecular modelling to the acquired data. From the molecular modelling, myricetin coordinated to the NPA cations by binding mode B could likely adopt two different poses, which may account for the deficient electron density map of myricetin, a potent PA endonuclease inhibitor.

In the second set of flavonoid derivatives, 24 compounds were tested by AlphaScreen assay. Out of those, orientin, the C-8-glucoside of luteolin exhibited IC_{50} of 42 nM. To assess the inhibition of endonuclease activity by selected compounds by a direct mechanism-based method, we applied a gel-based endonuclease inhibitory assay. This assay was performed for five selected ligands with wild-type. The analysis showed that orientin had a higher inhibitory potency than luteolin, which corresponded to the AlphaScreen assay. The gel-based assay also confirmed similar inhibition activities for baloxavir acid, and orientin. We also attempted this assay with the NPA I38T variant, but the mutation of Ile-38 to Thr-38 led to complete loss of ssDNA cleavage ability. Thus, we used a fluorescent-labelled ssRNA substrate and performed a FRET-based endonuclease assay with this variant. Compared to wild-type NPA, the I38T variant had only 1.9% activity toward the ssRNA substrate and none for ssDNA.

To reveal the structure of orientin bound to wild-type NPA and the I38T mutant, we have crystallized both proteins and soaked in orientin. The structure of complex of the wild-type NPA/orientin was refined to 1.9 Å resolution (PDB ID **7NUG**), and the I38T mutant complex (PDB ID **7NUH**) was refined to 2.2 Å resolution. Both crystallographic models consisted of one protein molecule per asymmetric unit. Two metal ions were embedded in the endonuclease active site. The ligand position within the active site was comparable to the previously published (**Figure 5B.**). The previously observed high affinity of luteolin for NPA was likely to be enhanced by the additional hydrogen bonding network surrounding orientin's glucosyl moiety. This was observed in both protein variants, as most of the water molecules in the first solvation shell are located at similar positions. However, there is a little ligand shift visible in the mutant variant. Wild-type Ile-38 moves orientin towards the solvent and differs from the mutant variant with an RMSD of 0.466 Å. Moreover, there is a visible movement of the Tyr-24 side chain in the mutant variant, likely to be due to the ligand shift. The side chain of Tyr-24 in the mutant variant approaches the active site pocket, whereas in the wild-type, Tyr-24 is pushed away from the cavity (RMSD of 0.029 Å for side chain atoms). Thr-38, which is one atom shorter than Ile-38, helps accommodate orientin. $O^{\gamma 1}$ Thr-38 forms a hydrogen bond through W21 to the glucosyl moiety of the ligand (O6). This is not observed in the wild-type, as Ile-38 does not contain a hydroxyl group capable of such interaction.

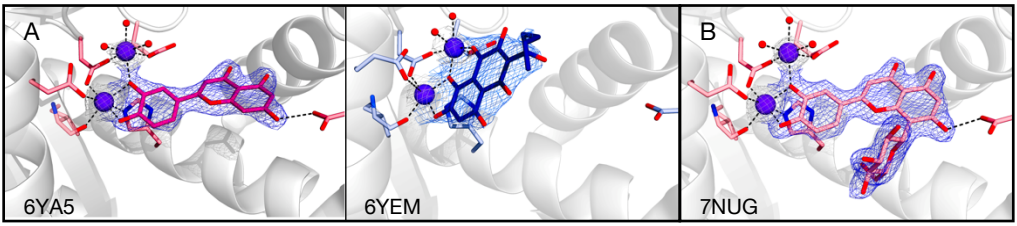

Figure 5. Close-up view onto the NPA endonuclease active sites. A) Two structures of luteolin (left) and quambalarine B (right) chelating the Mn^{2+} ions. **B)** Orientin displaying similar binding mode as luteolin. PDB codes are in the down-left corner. The 2*F*o - *F*c electron density maps (contoured at 1.5σ) are as a blue mesh.

CONCLUSION AND DISCUSSION

As influenza remains a serious viral infection with pandemic potential, searching for a new antiviral drug is ongoing. Several viral drug targets have been identified. We have focused on two targets placed within the heterotrimeric influenza RNA-dependent RNA polymerase, both within the PA subunit.

The intersubunit PA-PB1 interaction, located on the C-terminus of PA, is a highly conserved region. Moreover, this PPI is essential for the heterotrimer assembly, therefore the viral cycle itself. As the first structure of PB1 N-terminus derived peptide was crystallized within the CPA binding pocket, we have started a project to explore the peptide and its derivates PPI inhibitory potency. Generally, the development of PPI inhibitors represents challenging targets for small-molecule inhibitors as the shared interface is most often wide and flat. However, this interaction is formed by a quite small hydrophobic pocket and an oligopeptide forming a 3_{10} helix. As the wild-type PA N-terminus derived peptide was 14 amino acids long (**PB1-0**, MDVNPTLLFLKIPA), we generated, and in publication **I.** analyzed a truncation peptide set by sequentially removing amino acids from each terminus. We expressed, purified influenza A CPA, and developed a high-throughput screening assay that enabled the biochemical characterization and determination of potent PA-PB1 peptide inhibitors. In the first generation of peptides, the truncation from both the C-terminus and the N-terminus exposed the oligopeptide interacting core and confirmed the importance of the internal 3_{10} helix. Truncation of the C-terminus amino acids was tolerated up to the Lys-11. When the peptide was cut shorter, the IC_{50} value worsened dramatically. Analogously we truncated the N-terminus up to Pro-5. These deletions were tolerated only to Asn-2, otherwise the half-maximal inhibitory concentration dropped in the order of magnitude. Minimal peptide **PB1-10** (DVNPTLLFLK) was identified as a low micromolar inhibitor (IC_{50} = 3 400 nM). Being inspired by a published peptide array, we introduced substitutions at “hot-spots” to enhance peptide affinity. Two substitutions (V3Y and T6Y) improved the inhibition activity, resulting in decapeptide **PB1-11** (DYNPYLLFLK) of IC_{50} of 13 nM. To evaluate if the decapeptide binding is structurally consistent with the wild-type, I have co-crystallized the CPA with this inhibitor. Crystals of CPA/**PB1-11** diffracted up to 1.6 Å resolution in $P\ 2_12_12_1$ symmetry. **PB1-11** was located at nearly the same position as the wild-type PB1-derived peptide. This high-resolution crystal

structure also revealed a structural basis for the affinity increase. The introduction of two tyrosine residues into the inhibitor sequence resulted in the formation of two water-mediated hydrogen bonds with the CPA Cys-415, Arg-638, Ser-659, and Asn-703. This was not observed for the wild-type peptide of PB1. We have also tried to improve the intracellular delivery of peptides. For this, we have joined the **PB1-11** peptide with the commonly used cell-penetrating Tat-sequence. However, this strategy did not help to deliver the linear decapeptide inside the cell and therefore failed to have an antiviral effect *in vivo*. This might also be due to the cell lines used in the assay. HEK293T and MDCK are generally known to struggle with cell-penetrating peptide-based delivery.

To follow up on the results from publication **I.**, we further modified and optimized the decapeptide to enhance its inhibitory potency and intracellular delivery in publication **II.**. Although many of the prepared oligopeptides were tested as nanomolar inhibitors, there were several subsequent issues needed to be overcome. Not mentioned above, the solubility of the first peptide set was very poor. Truncated, modified peptides, as well as the native **PB1-0** peptide, precipitated/aggregated in higher concentrations in an aqueous solution. We prepared a second set of decapeptides with modified hot-spots. One modification of all three hot-spots led to a decapeptide **PB1-19** (DYNPYLLYLK) with IC_{50} of 5.5 nM. Its maximal solubility was over 200 μM. This enabled us to perform the first thermodynamic analysis of the PA-PB1 peptide inhibitor. The binding of **PB1-19** to the CPA was enthalpy-driven with a dissociation constant K_D of 1.7 nM. This suggested a high degree of van der Waals interactions and favorable hydrogen bonding between the decapeptide and CPA. Conformational changes which are coupled to the binding process resulted in unfavorable entropy change. I have co-crystallized the protein-decapeptide complex. Crystals of CPA/**PB1-1**9 diffracted up to 1.9 Å resolution again in the $P\ 2_12_12_1$ symmetry. Using the X-ray crystallography, I have found additional water-mediated hydrogen bonds in the binding pocket (PDB code **7ZPY**), compared to the previously described decapeptide **PB1-11** (PDB code **6SYI**). These new water molecules binding between the CPA and hydroxyl from the introduced F9Y side chain shifted two CPA alpha helices α11 and α12 of RMSD of 0.84 Å for corresponding 332 atoms. To improve peptide intracellular delivery, we have employed a reversible bicyclic strategy approach. Both peptides **PB1-11** and **PB1-19** were fused with a short CPP

motif (cyclo(RRRRØF), where Ø is L-2-naphtylalanine) and formed into the bicyclic peptide by the creation of two disulfide bonds. Hypothetically, the bicyclic peptide **PB1-11B**/**PB1-19B** would enter the cell via endocytosis and escape the early endosome into the cytosol. A PA-PB1 inhibiting linear peptide would be then released after the intracellular glutathione reduces the pair of disulfide bonds. To observe the peptide delivery, we have labelled the **PB1-11** and **PB1-11B** with rhodamine B (RB) and naphtofluororescein (NF). We have treated HeLa cells with those peptides and visualized them on the confocal microscope. The pH-insensitive RB-labelled peptides were observed through the entire range of pH. But the fluorescence of NF-labelled peptides was detected only in the cytosol, due to the pH sensitivity of the label. Comparing labelled linear and bicyclic peptides, the formation of bicyclic peptides enhanced the transmembrane transport, as well as the escape from the early endosome. We have further characterized the effect of bicyclic peptides targeting PA-PB1 interaction in cell cultures. Two approaches applied on HEK293T and MDCK cell lines, the mini-replicon assay and the cytopathic effect (CPE) reduction assay were used. In both, the introduction of the bicyclic strategy improved the inhibitory potency of bicyclic peptides. The PB1-19B was determined as a low micromolar RdRp inhibitor (EC_{50} of 1 μM, 2 μM respectively). All peptides were cell-tolerated up to 100 μM concentration. Moreover, the peptides were tested for their stability in human plasma. The bicyclization prolonged the peptide's half-lives over ten times.
To conclude the CPA project, we developed a novel high-throughput method and tested two sets of peptide-based inhibitors of the PA-PB1 interaction. We optimized a selected decapeptide and structurally characterized its binding into the CPA pocket. This resulted in two structures of protein-peptide complexes with PDB codes **6SYI** and **7ZPY**. Thanks to the increased solubility of **PB1-19**, the very first ITC of this interaction was performed. In combination with the reversible bicyclic strategy, we have significantly improved the peptide stability and inhibition in cell-based assays. This could provide a starting point for a structure-based development of compounds targeting the protein-protein interaction between PA and PB1 subunits.

Our second project was focused on the PA endonuclease domain, located at the N-terminus (NPA). This domain can be considered a first-thought drug target, as it

is a bridged metalloenzyme with a solvent-exposed binding pocket. Several compounds were designed to chelate the two manganese ions in the active site. Promising NPA inhibitors include the phytochemicals from the catechol derivatives, such as the epigallocatechin gallate (EGCG) and its congener epicatechin gallate. Both are contained in green tea and have exhibited some inhibitory potency against endonuclease activity. Other flavonoids share some structural similarities with EGCG. From the protein-inhibitor crystal structure (**4AWM**, Kowalinski et al., 2012), we have considered compounds of this class as promising compounds to target NPA. Besides being part of a daily diet, flavonoids were studied for their potential benefits for human health. One of them, quercetin was described to have some inhibitory effect on viruses including influenza. Several in vitro and in vivo experiments in mice had been previously performed. However, no structure-based proof of protein target was revealed. To test if quercetin and its derivatives act on the NPA, we have prepared DNA encoding the first 196 amino acids of NPA. The sequence was optimized for crystallization as a flexible loop region was replaced by a GGS linker. We have expressed the NPA domain and purified it. For the testing of prepared compounds, we have developed a novel high-throughput AlphaScreen-based assay. This assay allowed us to confirm the NPA as a quercetin protein target. We have studied the SAR of flavonoids and their analogs in the endonuclease active site. A series of 83 compounds was prepared and tested (publication **III.**). The results from AlphaScreen were further verified by the in vitro cleavage endonuclease gel-based assay. To support our hypothesis, that the binding site is the endonuclease active site of the NPA, I have crystallized the NPA domain. When hexagonal bifrustum crystals were formed, luteolin, quambalarine B, and myricetin were soaked in. Due to the flavonoid's natural colorful character, the crystal color change could be observed over time. All crystals belonged to the $P\,6_422$ space group and had a clear anomalous signal. Crystal of NPA/luteolin complex diffracted up to 2.0 Å and NPA/quambalarine B up to 2.5 Å. Luteolin chelated the manganese ions in a bidentate binding mode **A** and formed an additional hydrogen bond via hydroxyl at C7 to the NPA Glu-26. On the other hand, quambalarine B exhibited the tridentate binding mode **B**. Atomic coordinates and experimental structure factors were deposited in the Protein Data Bank under codes **6YA5** and **6YEM**. I obtained crystal structures of NPA in complex with luteolin and quambalarine B. The

position of myricetin could not be determined from the electron density map. This was maybe due to myricetin flexibility within the active site. We have used rough estimates of myricetin position from the X-ray structure for molecular modelling. To conclude, we found that flavonoids target the NPA domain of influenza RdRp. Furthermore, we established a novel method for high-throughput screening assay, which was correlated to the gel-based assay. For the first time, we identified the molecular mode-of-action of flavonoids bound to the endonuclease active site of the influenza RdRp. This could be a set off in a rational design of the NPA endonuclease next-generation inhibitors.

We continued to map the protein chemical space around the flavonoid ligand. In publication **IV.**, we studied the next generation of luteolin-derived compounds. Specifically changes at the C-7 and C-8 positions. Another set of 24 prepared compounds was tested for its inhibitory potency of NPA endonuclease. Analogously to the previous work, we have utilized the AlphaScreen technology, as well as the generally used gel-based in vitro endonuclease cleavage assay. Moieties introduced to the C-7 position did not have any advantageous effect on the inhibitory potency. The C-8 derivatives exhibited generally decent submicromolar half-maximal inhibitory concentration. The most promising NPA inhibitor of the set was orientin (IC_{50} of 42 nM), a C-8-glucose derivative of luteolin. In patients, a point mutation I38T of NPA within the active site was observed, as a response to the treatment with an FDA-approved endonuclease inhibitor Xofluza (baloxavir marboxil). Therefore, we included this mutant variant in the endonuclease assay. We found out that this mutation in the endonuclease active site led to a complete loss of ssDNA cleavage ability. Nevertheless, the influenza polymerase is RNA-dependent. We have used a fluorescent-labelled ssRNA substrate for a FRET-based endonuclease assay to test the ssRNA cleavage. Compared to the wild-type NPA, the I38T variant had only 1.9% activity toward the ssRNA substrate. This observation was in correlation with a report of significantly reduced fitness and ssRNA nuclease activity of a virus carrying the I38T mutation. To characterize orientin in the active site, I have crystallized the protein of wild type NPA along with the I38T mutant variant. Both protein crystals exhibited the same $P\,6_422$ symmetry. Orientin was consequently soaked into empty crystals in a short period of time. The complex of wild type NPA/orientin diffracted up to 1.9 Å resolution (**7NUG**), and I38T/orientin up to 2.2 Å resolution (**7NUH**).

In both structures, the ligands were clearly visible with the electron density map well defined. Orientin was bound to two manganese ions almost identically to the luteolin scaffold in our previous structure. It also remained the C-7 hydroxyl-mediated hydrogen bond to the Glu-26. The introduction of the I38T mutation did not lead to any major changes in the binding mode of orientin. The enhanced affinity of orientin was likely due to the additional hydrogen bonding network surrounding orientin's glucosyl moiety. This was observed in both protein variants as a vast majority of the water molecules in the first solvation shell were located at similar positions. One of only two differences was a small ligand shift in the mutant variant with an RMSD of 0.446 Å. The second one was an evident movement of Tyr-24. Its side chain was pushed away from the cavity with an RMSD of 0.029 Å. The Thr-38 is one atom shorter than Ile-38 and better lodged the inhibitor in the active site and formed an additional hydrogen bond to an extra water molecule via its $O^{\gamma 1}$. This suggested that this clinically relevant mutation should not affect the orientin binding into the NPA endonuclease domain.

To conclude, the presented publications in this dissertation closely examine two different drug targets located within the influenza PA subunit. I must mention that I was lucky to obtain six X-ray structures with bound inhibitors altogether. This contributed to a detailed exploration of their interactions with binding sites of protein targets and follow up optimizations. Optimized minimal peptidic inhibitors derived from the PB1 subunit were found to be potent RdRp inhibitors. Any of the peptide-based inhibitors are considered as an attractive alternative to small molecule drugs. They can be specific, more efficient, and most importantly better tolerated. Generally, to translate peptide-based inhibitors into clinical application, they must be potent, stable, and have good bioavailability. Improving these features may lead to a highly potent anti-influenza drug. One way to obtain such compound could be through their cyclization, which should possibly prevent their degradation in human plasma. This modification can also be considered as a first step towards synthetic inhibitor specifically targeting a viral protein. However, the peptide cyclization can negatively affect its inhibitory potency, as the binding site in the PA subunit is relatively closed. Another approach for an intracellular delivery and stability enhancement could be using a carrier systems, such as nanoparticles with inhibitory peptides as a cargo. A different way is the utilization of chemically synthesized non-peptidic compounds, which mimic the 3_{10} helix structure.

Nonetheless, such inhibitor might act differently, and may not be advantageous for intracellular delivery. Altogether, any of the suggested compounds can stand a chance in the development of novel influenza virostatics and could be classed beside other currently used therapeutic peptides.

Biological effects of substances obtained from plants have been known for centuries. Natural products represent a huge reservoir of bioactive chemical diversity and a potential drug leading to new therapeutics for many human diseases. One class, the flavonoids, showed beneficial effects on the human health. Beside many others, the antiviral effect was mentioned. Although there were several proposals of their mechanism of action, there was no clear consensus for the protein target. For the first time, we present the structural characterization of this plant-derived compound as a nonspecific influenza inhibitor. Luteolin and its derivatives inhibit the influenza endonuclease by chelating its embedded metal ions. These observations of the active site with bound flavonoids may serve for the development of more potent influenza RdRp endonuclease inhibitors derived from this scaffold.

RNA viruses typically adapt rapidly to new hosts. Their mutation rate is high, also caused by the impreciseness of the RNA-dependent RNA polymerase, which is prone to translation and replication errors. From past pandemics, it is clear that the emergence of antiviral-resistant influenza viruses is not easily predictable. The development of virostatics against all RNA viruses would need to be considered a suitable target. So far, the RdRp appears to be one of the promising ones. The above-presented targets in the PA subunit have the advantage of their essential role within the viral life cycle, and the C-terminal PPI is especially suitable for its highly conserved region within influenza viruses. The general therapeutic nucleoside analogue, favipiravir, targets not only influenza viruses. Though, it has severe negative side effects and did not pass the development of resistant mutations. It might be that a universal virostatic recquires a different approach. One of those may represent the targeted protein degradation or a novel class of optimized nucleoside analogues.

SUMMARY

Influenza virus causes acute infection of the respiratory system among humans and presents a year-round disease burden. As the influenza virus is constantly mutating and has pandemic potential, new antiviral drugs need to be developed. Currently used antivirals in the majority target the viral surface protein neuraminidase and are used with limitations. In the past twenty years, several viral drug targets have been identified. This thesis focuses on the two of them, both located within the viral heterotrimeric RNA-dependent RNA polymerase (RdRp). The first is the PA subunit C-terminal domain (CPA) harboring the protein protein interaction (PPI) with the PB1 subunit. The second is the PA subunit N-terminal domain (NPA), carrying the endonuclease active site. Revealing their structure with novel inhibitors would bring new aspects to rational structure-based drug development.

The PA-PB1 PPI is mediated by the small 3_{10} helix from the PB1 N-terminus inside the CPA hydrophobic pocket. The structure with a 25 amino acids long peptide inhibiting the assembly of RdRp heterotrimer was previously published. Therefore, we have decided to map the chemical space around the peptide,and to truncate and modify the peptide inhibitor maintaining the inhibitory potency. To study the first set of peptide inhibitors, we expressed the CPA domain and developed an AlphaScreen assay. Utilizing this assay, we tested ten peptides and selected one peptide to be modified according to the peptide array. This resulted in a nanomolar inhibitory potency of peptide **PB1-11** (DYNPYLLFLK), and a high-resolution crystal structure of the CPA with bound peptide (publication **I.**). However, using the generally used cell-penetrating Tat sequence connected to the peptide inhibitor did not improve the intracellular delivery of the inhibitory peptide. Therefore, the antiviral in vivo effect was not observed. To overcome this, we have further employed the recently published strategy, where the bicyclic peptide contains a cell-penetrating peptide in one cycle and the inhibitor peptide in the other cycle. The bicyclic strategy improved the intracellular delivery, and we were able to observe the peptide endosomal escape. Moreover, we have optimized the **PB1-11** peptide to the final **PB1-19** peptide (DYNPYLLYLK), resulting in a vastly improved solubility of the peptide in higher concentrations, allowing the first isothermal titration calorimetry (ITC) of this PA-PB1 interaction (publication **II.**). The **PB1-19** peptide was characterized as a low nanomolar inhibitor of the PA-PB1 PPI and was also observed from the X-ray protein crystallography data within the

hydrophobic pocket of the CPA. These results may serve as a starting point for further peptide optimization or the design of non-peptidic PA-PB1 PPI inhibitors.
The NPA endonuclease is essential for viral transcription, as it cleaves the primer from host mRNA. The enzyme embeds two solvent-exposed metal ions in the active site. Currently, there is one FDA approved compound, the baloxavir marboxil (BAM), targeting the NPA endonuclease. In the other part of this thesis, we were exploring the inhibitory potency of phytochemicals flavonoids and their derivatives against the NPA endonuclease domain. We have developed a high-throughput assay and tested over 80 compounds. Some of them were characterized as submicromolar inhibitors of the NPA, including luteolin and quambalarine B. The NPA endonuclease was identified as the target protein of those compounds which are broadly used as supplements during influenza viral infection. We crystallized the NPA with selected compounds and observed two binding modes (bidentate and tridentate) of the compounds to the metal ions in the active site. The molecular mode-of-action of flavonoids towards the influenza virus was revealed for the first time (publication **III.**). We continued to explore the structure-activity relationship (SAR) of luteolin derivatives. The second set of 21 compounds was prepared and tested. Orientin is a luteolin derivative with the C-8 introduced glucose moiety. It was characterized as a nanomolar inhibitor of the NPA endonuclease. Its glucose moiety formed an additional water-mediated net of hydrogen bonds, while maintaining the luteolin binding mode. Moreover, we prepared a mutant variant carrying the substitution of Ile-38 to Thr-38, which emerged during the BAM clinical trials. Although it reduced the susceptibility to BAM 30- to 50-fold, it did not affect the binding of orientin to the NPA. From the analyses of the I38T mutant variant crystal structure, the mutation occurred at a distant region of the endonuclease active site (publication **IV.**). Even though subsequent optimizations of the chemical structure of the flavonoid derivatives are needed to enhance their bioavailability, the protein-compound structure analysis brought additional insights into the protein inhibitor interactions.

SOUHRN

Virus chřipky způsobuje akutní infekci respiračního systému u lidí a představuje riziko onemocnění v rámci celého roku. Jelikož virus chřipky neustále mutuje a zároveň má pandemický potenciál, je potřeba vyvíjet stále nová antivirotika. V současnosti se většinou používají léky cílící na povrchový protein viru, neuraminidasu, a jsou užívány s určitou limitací. V posledních dvaceti letech bylo na viru identifikováno několik možných cílů pro antivirotické léky. Tato práce se zaměřuje na dva z nich, oba obsažené ve virové RNA-dependentní RNA polymerase (RdRp). Prvním z nich je C-koncová doména PA podjednotky (CPA) obsahující protein-proteinovou interakci (PPI) s podjednotkou PB1. Druhým z nich je N-koncová doména PA podjednotky (NPA), která obsahuje endonukleasovou doménu. Pokud by se získala jejich trojrozměrná struktura s navázaným inhibitorem, přineslo by to důležitý poznatek do racionálního vývoje léků založeného na struktuře.

PPI mezi PA a PB1 podjednotkou je zprostředkovaná malým 3_{10} helixem, odvozeným z N koncové části PB1 podjednotky, který se váže do hydrofobní kapsy uvnitř CPA. Již dříve byla zveřejněna struktura peptidu dlouhého 25 aminokyselin, který inhiboval zkompletování celého RdRp heterotrimeru. Na základě této práce jsme se rozhodli zmapovat chemický prostor kolem peptidu a dále zkrátit a upravit peptidový inhibitor tak, aby si stále zachoval inhibiční potenci. V bakteriích jsme vyprodukovali CPA doménu, abychom mohli studovat první sérii peptidových inhibitorů, a zároveň vyvinuli AlphaScreen metodu na testování inhibitorů. Pomocí této metody jsme testovali deset peptidů, z nichž jsme jeden dále modifikovali. Výsledkem byl nanomolární peptidový inhibitor **PB1-11** (DYNPYLLFLK). Z krystalu komplexu s CPA jsme byli schopni určit jejich strukturu ve vysokem rozlišení (publikace **I.**). Ačkoliv jsme využili obecně používanou metodu, kdy se na peptid připojí Tat sekvence, nezlepšil nám tento přístup přenos peptidu přes buněčnou membránu. Kvůli špatné biologické dostupnosti jsme nepozorovali antivirový efekt in vivo. Abychom obešli prostupnost inhibitorů přes membránu, použili jsme nedávno publikovanou strategii využívající bicyklické peptidy. Jeden cyklus je tvořený peptidovou sekvencí, která prostupuje buněčnou membránou a druhý, který nese sekvenci peptidového inhibitoru. Tento příštup zlepšil dostupnost peptidového inhibitoru do buňky a zároveň jsme byli schopni sledovat únik peptidu z endosomu. Dále jsme optimalizovali **PB1-11** peptid na výsledný peptid **PB1-19**

(DYNPYLLYLK), který byl daleko rozpustnější, což nám umožnilo vůbec první mikrokalorimetrickou charakterizaci vazby inhibitoru PA-PB1 interakce pomocí isotermální titrační kalorimetrii (ITC) (publikace **II.**). Peptid **PB1-19** byl charakterizován jako nanomolární inhibitor PA-PB1 PPI, a současně jsme získali trojrozměrnou strukturu s CPA pomocí rentgenové krystalografie. Tyto výsledky mohou sloužit jako výchozí bod pro další optimalizaci peptidu, nebo pro design nepeptidových inhibitorů PA-PB1 interakce.

Endonukleasa v N-koncové části PA podjednotky (NPA) je nezbytná pro transkripci viru, jelikož vytváří primer z mRNA hositelské buňky. V aktivní části enzymu jsou usazené dva kovové ionty, které jsou vystavené do solventu. V současné době je dostupná jedna látka cílící na NPA endonukeasu, baloxavir marboxil (BAM). V druhé části disertační práce jsme zkoumali inhibiční možnosti rostlinných látek flavonoidů a z nich odvozených sloučenin proti NPA endonukleasové doméně. Vyvinuli jsme esej pro vysokokapacitní testování sloučenin a pomocí ní otestovali přes 80 látek. Některé z nich byly charakterizované jako submikromolární inhibitory NPA, včetně luteolinu a quambalarinu B. NPA endonukleasa byla identifikovaná jako cílový protein těchto sloučenin, které jsou běžně užívané při infekci způsobené virem chřipky. Povedlo se nám vykrystalizovat NPA protein s vybranými sloučeninami a ze struktury jsme identifikovali dva vazebné módy látek na kovové ionty v aktivním místě enzymu. Tímto jsme poprvé odhalili molekulární podstatu vazby flavonoidů proti viru chřipky (publikace **III.**). Nadále jsme pokračovali s prozkoumáváním vztahu mezi strukturou a aktivitou derivátů luteolinu. Připravili jsme a otestovali druhou série o 21 sloučeninách. Orientin je derivát luteolinu, který má na uhlíku C-8 glukosový zbytek. Byl charakterizovaný jako nanomolární inhibitor NPA endonukleasy. Glukosová část tvoří dodatečnou síť vodíkových vazeb s vedlejšími řetězci v aktivním místě, zprostředkovanou molekulami vody, zatímco si zachovává obdobný vazebný mód jako luteolin. V klinických studiích BAM se objevila varianta NPA proteinu, která nese substituci Ile-38 na Thr-38, a která zhoršila citlivost viru na BAM inhibitor 30- až 50-krát. Variantu I38T jsme rovněž připravili a otestovali, ale nijak neovlivnila vazbu orientinu do NPA aktivního místa. Z analýzy krystalové struktury vyplývá, že se mutace nachází na odlehlém místě aktivního místa endonukleasy od vazebného místa orientinu (publikace **IV.**). Další optimalizace chemické struktury flavonoidových derivátů budou potřeba,

aby se zlepšila jejich biodostupnost. I přesto přinesla analýza struktur komplexu proteinu se sloučeninami nová porozumění jejich vzájemných interakcí.

REFERENCES

Arranz, R., Coloma, R., Chichón, F. J., Conesa, J. J., Carrascosa, J. L., Valpuesta, J. M., Ortín, J., & Martín-Benito, J. (2012). The Structure of Native Influenza Virion Ribonucleoproteins. *Science*, *338*(6114), 1634–1637. https://doi.org/10.1126/science.1228172

Bailey, S. (1994). The CCP4 suite: programs for protein crystallography. *Acta Crystallographica Section D Biological Crystallography*, *50*(5), 760–763. https://doi.org/10.1107/S0907444994003112

Barman, S., Adhikary, L., Chakrabarti, A. K., Bernas, C., Kawaoka, Y., & Nayak, D. P. (2004). Role of Transmembrane Domain and Cytoplasmic Tail Amino Acid Sequences of Influenza A Virus Neuraminidase in Raft Association and Virus Budding. *Journal of Virology*, *78*(10), 5258–5269. https://doi.org/10.1128/JVI.78.10.5258-5269.2004

Cady, S. D., Luo, W., Hu, F., & Hong, M. (2009). Structure and function of the influenza A M2 proton channel. *Biochemistry*, *48*(31), 7356–7364. https://doi.org/10.1021/bi9008837

Emsley, P., & Cowtan, K. (2004). Coot : model-building tools for molecular graphics. *Acta Crystallographica Section D Biological Crystallography*, *60*(12), 2126–2132. https://doi.org/10.1107/S0907444904019158

Gottschalk, A. (1957). Neuraminidase: the specific enzyme of influenza virus and Vibrio cholerae. *Biochimica et Biophysica Acta*, *23*(C), 645–646. https://doi.org/10.1016/0006-3002(57)90389-X

He, X., Zhou, J., Bartlam, M., Zhang, R., Ma, J., Lou, Z., Li, X., Li, J., Joachimiak, A., Zeng, Z., Ge, R., Rao, Z., & Liu, Y. (2008). Crystal structure of the polymerase PA(C)-PB1(N) complex from an avian influenza H5N1 virus. *Nature*, *454*(7208), 1123–1126. https://doi.org/10.1038/nature07120

Hejdánek, J., Radilová, K., Pachl, P., Hodek, J., Machara, A., Weber, J., Řezáčová, P., Konvalinka, J., & Kožíšek, M. (2021). structural characterization of the interaction between the C-terminal domain of the influenza polymerase PA subunit and an optimized small peptide inhibitor. *Antiviral Research*, *185*(August 2020), 104971. https://doi.org/10.1016/j.antiviral.2020.104971

Kabsch, W. (2010). XDS. *Acta Crystallographica Section D Biological Crystallography*, *66*(2), 125–132. https://doi.org/10.1107/S0907444909047337

Kowalinski, E., Zubieta, C., Wolkerstorfer, A., Szolar, O. H. J., Ruigrok, R. W. H., & Cusack, S. (2012). Structural Analysis of Specific Metal Chelating Inhibitor Binding to the Endonuclease Domain of Influenza pH1N1 (2009) Polymerase. *PLoS Pathogens*, *8*(8), e1002831. https://doi.org/10.1371/journal.ppat.1002831

Krug, M., Weiss, M. S., Heinemann, U., & Mueller, U. (2012). XDSAPP: A graphical user interface for the convenient processing of diffraction data using XDS. *Journal of Applied Crystallography*, *45*(3), 568–572. https://doi.org/10.1107/S0021889812011715

Lovell, S. C., Davis, I. W., Arendall, W. B., de Bakker, P. I. W., Word, J. M., Prisant, M. G., Richardson, J. S., & Richardson, D. C. (2003). Structure validation by

Cα geometry: ϕ,ψ and Cβ deviation. *Proteins: Structure, Function, and Bioinformatics*, *50*(3), 437–450. https://doi.org/10.1002/prot.10286

Machara, A., Lux, V., Kožíšek, M., Grantz Šašková, K., Štěpánek, O., Kotora, M., Parkan, K., Pávová, M., Glass, B., Sehr, P., Lewis, J., Müller, B., Kräusslich, H.-G., & Konvalinka, J. (2016). Specific Inhibitors of HIV Capsid Assembly Binding to the C-Terminal Domain of the Capsid Protein: Evaluation of 2-Arylquinazolines as Potential Antiviral Compounds. *Journal of Medicinal Chemistry*, *59*(2), 545–558. https://doi.org/10.1021/acs.jmedchem.5b01089

Mueller, U., Förster, R., Hellmig, M., Huschmann, F. U., Kastner, A., Malecki, P., Pühringer, S., Röwer, M., Sparta, K., Steffien, M., Ühlein, M., Wilk, P., & Weiss, M. S. (2015). The macromolecular crystallography beamlines at BESSY II of the Helmholtz-Zentrum Berlin: Current status and perspectives. *The European Physical Journal Plus*, *130*(7), 141. https://doi.org/10.1140/epjp/i2015-15141-2

Murshudov, G. N., Vagin, A. A., & Dodson, E. J. (1997). Refinement of Macromolecular Structures by the Maximum-Likelihood Method. *Acta Crystallographica Section D Biological Crystallography*, *53*(3), 240–255. https://doi.org/10.1107/S0907444996012255

Qian, Z., Rhodes, C. A., McCroskey, L. C., Wen, J., Appiah-Kubi, G., Wang, D. J., Guttridge, D. C., & Pei, D. (2017). Enhancing the Cell Permeability and Metabolic Stability of Peptidyl Drugs by Reversible Bicyclization. *Angewandte Chemie - International Edition*, *56*(6), 1525–1529. https://doi.org/10.1002/anie.201610888

Reich, S., Guilligay, D., Pflug, A., Malet, H., Berger, I., Crépin, T., Hart, D., Lunardi, T., Nanao, M., Ruigrok, R. W. H., & Cusack, S. (2014). Structural insight into cap-snatching and RNA synthesis by influenza polymerase. *Nature*, *516*(7531), 361–366. https://doi.org/10.1038/nature14009

Song, M.-S., Kumar, G., Shadrick, W. R., Zhou, W., Jeevan, T., Li, Z., Slavish, P. J., Fabrizio, T. P., Yoon, S.-W., Webb, T. R., Webby, R. J., & White, S. W. (2016). Identification and characterization of influenza variants resistant to a viral endonuclease inhibitor. *Proceedings of the National Academy of Sciences*, *113*(13), 3669–3674. https://doi.org/10.1073/pnas.1519772113

Vagin, A., & Teplyakov, A. (2000). An approach to multi-copy search in molecular replacement. *Acta Crystallographica Section D Biological Crystallography*, *56*(12), 1622–1624. https://doi.org/10.1107/S0907444900013780

Webster, R. G., Laver, W. G., Air, G. M., & Schild, G. C. (1982). Molecular mechanisms of variation in influenza viruses. *Nature*, *296*(5853), 115–121. https://doi.org/10.1038/296115a0

Wunderlich, K., Juozapaitis, M., Ranadheera, C., Kessler, U., Martin, A., Eisel, J., Beutling, U., Frank, R., & Schwemmle, M. (2011). Identification of High-Affinity PB1-Derived Peptides with Enhanced Affinity to the PA Protein of Influenza A Virus Polymerase. *Antimicrobial Agents and Chemotherapy*, *55*(2), 696–702. https://doi.org/10.1128/AAC.01419-10

PUBLICATIONS INCLUDED

I. Hejdanek, J., Radilova, K., Pachl, P., Hodek, J., Machara, A., Weber, J., Rezacova, P., Konvalinka, J., and Kozisek, M.; 2021. "**Structural Characterization of the Interaction between the C-Terminal Domain of the Influenza Polymerase PA Subunit and an Optimized Small Peptide Inhibitor**." *Antiviral Research* 185 (January 2021): 104971. doi: 10.1016/j.antiviral.2020.104971. **$IF_{(2021)}$ = 10.19**

II. Radilova, K., Zima, V., Kral, M., Machara, A., Majer, P., Hodek, J., Weber, J., Brynda, J., Strmen, T., Konvalinka, J., and Kozisek, M. 2022. "**Thermodynamic and structural characterization of an optimized peptide-based inhibitor of the influenza polymerase PA-PB1 subunit interaction.**" *Antiviral Research* 208 (December 2022): 105449. doi: 10.1016/j.antiviral.2022.105449. **$IF_{(2021)}$ = 10.19**

III. Zima, V.*, Radilova, K.*, Kozisek, M., Albinana, C. B., Karlukova, E., Brynda, J., Fanfrlik, J., Flieger, M., Hodek, J., Weber, J., Majer, P., Konvalinka, J., and Machara, A.; 2020. "**Unraveling the Anti-Influenza Effect of Flavonoids: Experimental Validation of Luteolin and Its Congeners as Potent Influenza Endonuclease Inhibitors.**" *European Journal of Medicinal Chemistry* 208:112754. doi: 10.1016/j.ejmech.2020.112754. **$IF_{(2020)}$ = 6.18**

IV. Reiberger, R.*, Radilova, K.*, Kral, M., Zima, V., Majer, P., Brynda, J., Dracinsky, M., Konvalinka, J., Kozisek, M., and Machara, A.; 2021. "**Synthesis and In Vitro Evaluation of C-7 and C-8 Luteolin Derivatives as Influenza Endonuclease Inhibitors.**" *International Journal of Molecular Sciences* 22(14):7735. doi: 10.3390/ijms22147735. **$IF_{(2021)}$ = 6.01**

PUBLICATIONS NOT INCLUEDED

I. Gregor, J., Radilova, K., Brynda, J., Fanfrlik, J., Konvalinka, J., and Kozisek M.; 2021. "**Structural and Thermodynamic Analysis of the Resistance Development to Pimodivir (VX-787), the Clinical Inhibitor of Cap Binding to PB2 Subunit of Influenza A Polymerase.**" *Molecules* 26 (4):1007. doi: 10.3390/molecules26041007. **$IF_{(2021)}$ = 5.56**